Communication

High-Temperature Tensile Properties of Nano-Oxide Dispersion Strengthened Ferritic Steels Produced by Mechanical Alloying and Spark Plasma Sintering

XAVIER BOULNAT, DAMIEN FABREGUE, MICHEL PEREZ, MARIE-HÉLÈNE MATHON, and YANN DECARLAN

Oxide-dispersion strengthened (ODS) ferritic steels were produced by mechanical alloying and subsequent spark plasma sintering. Very fast heating rates were used to minimize porosity when controlling grain size and precipitation of dispersoids within a compacted material. Sintering cycles performed at 1373 K (1100 °C) induced heterogeneous, but fine grain size distribution and high density of nano-oxides. Yield strengths at room temperature and at 923 K (650 °C) are 975 MPa and 298 MPa, respectively. Furthermore, high-temperature ductility is much increased: total strain of 28 pct at 923 K (650 °C).

DOI: 10.1007/s11661-013-1719-6

Oxide-dispersion strengthened (ODS) ferritic–martensitic steels are foreseen as highly irradiated materials for fission and fusion reactors.[1–7] To enhance creep resistance, these materials are reinforced by dispersoids within the ferritic matrix. To do so, the elaboration route includes powder metallurgy where nanometric Yttria powder and prealloyed ferritic powder are mechanically alloyed. Then, Hot Isostatic Pressing (HIP) and/or hot extrusion (HE) are classical, almost unique, steps to consolidate the materials.[1–8] However, abnormal grain growth and precipitation coarsening are often observed as these processes induce long thermo-mechanical treatments, *i.e.*, often more than 2 hours at temperatures over 1273 K (1000 °C). Compared with HE or HIP, spark plasma sintering (SPS) spends much less time in both heating and cooling during sintering process. Thus, SPS has emerged because of its ability to heat up the material very quickly, providing a powerful tool to retain the original nanostructure.[9,10] For industrial purpose, it has been used for ceramics applications and refractory materials whereas only few studies were dedicated to metallic materials.[11] Very recently, G. Ji *et al.* demonstrated that SPS could be used to retain the nanostructure of ODS intermetallic alloys.[12,13] However, with bending tests, they highlighted the efforts that have to be done to improve ductility despite degassing treatments. The current study aims at investigating the SPS technique as a tool for the compaction of ODS ferritic steels. Under optimal sintering conditions, semi-industrial dense pellet (0.5 kg) of ODS ferritic steel can be processed in less than 20 minutes. The associated grain structure and precipitation state have been investigated and linked to the tensile behavior at various temperatures.

The powder was produced by Mechanical Alloying (MA) of a gas-atomized prealloyed steel Fe-14Cr-1W with Yttria powder (Y_2O_3) and TiH_2 powder. TiH_2 was used to add Titanium into the metallic matrix in order to refine the oxide dispersion during further processing.[14] The MA was made by high-energy attrition, dissolving the major part of Titanium, Yttrium and Oxygen in the matrix or into amorphous nanoparticles[4,15] and giving highly deformed granules with asymmetric shapes. The MA powder was then consolidated by SPS to form a dense cylindrical pellet of 60 mm diameter and 20 mm height. SPS device was a HP D 25 (FCT System, Germany). Various sintering cycles with different pressures and thermal cycles were used to get fully dense materials. The optimized compaction cycle for best relative density (0.98) consisted of a uniaxial loading of 215 kN (average pressure of 76 MPa) followed by a heating ramp of 300 K/min (300 °C/min) up to 1373 K (1100 °C), a holding stage of 5 minutes and finally a cooling down by direct contact with water-cooled punches. The temperature was controlled by a vertical pyrometer targeting inside the upper punch close to the powder, which is the reference in the current study, and a thermocouple set into the graphite die.

Chemical homogeneity of both MA powder and sintered samples was characterized by electron probe microanalysis using a device SX 100 CAMECA (Table I). Grain structure was characterized by a scanning electron microscope (SEM) Zeiss Supra 55 VP with field-emission gun (FEG), using either a high-current mode with low tension (3-5 kV), or an Electron BackScatter System (EBSD) at 15 kV with a step size of 50 nm. Small Angle Neutron Scattering (SANS) experiments were performed at the Laboratoire Léon Brillouin (CEA Saclay) using the same experimental settings as those described in Reference 14. Dog-bone tensile specimens had a gauge length of 6 mm and a cross section of 1.125 mm^2. Thanks to the pellet dimensions, they were machined in the same sintered ODS steel in both axial and radial directions. Mechanical tests were carried out at room temperature and at 873 K, 923 K, and 973 K (600 °C, 650 °C, and 700 °C) with a strain rate of 7×10^{-4} s^{-1} in a tensile machine Instron with a load cell of 2 kN and equipped with a radiation furnace. Temperature gradient onto the

XAVIER BOULNAT, Ph.D. Student, is with the CEA, DEN, Service de Recherches Métallurgiques Appliquées, 91191 Gif-sur-Yvette, France, and also with the Université de Lyon, INSA-Lyon, MATEIS UMR CNRS 5510, 69621 Villeurbanne, France. Contact e-mail: xavier.boulnat@cea.fr DAMIEN FABREGUE, Associate Professor, and MICHEL PEREZ, Professor, are with the Université de Lyon, INSA-Lyon, MATEIS UMR CNRS 5510. MARIE-HÉLÈNE MATHON, Researcher, is with the Laboratoire Léon Brillouin, CEA-CNRS, CEA/Saclay, 91191 Gif-sur-Yvette, France. YANN DE CARLAN, Researcher, is with the CEA, DEN, Service de Recherches Métallurgiques Appliquées.

Manuscript submitted January 7, 2013.
Article published online April 9, 2013

specimen was measured by thermocouple and did not exceed 2 K.

Using powder metallurgy to process structural materials requires a careful attention to the initial structure of the materials, as its evolution along the processing route definitely governs the final properties. Chemical composition profiles measured in powder grains showed at micronic scale a homogeneous repartition of each solute, especially Yttrium and Oxygen, as observed in Reference 5. This demonstrates that high-energy attrition equally distributed solutes into the ferritic matrix.[4,15] The specific heating system of the SPS device drastically influences the kinetics of thermally activated phenomena, such as grain growth and precipitation. Figure 1(a) illustrates the heterogeneous grain structure of the sintered ODS steel. Grains larger than 1 μm, and up to 20 μm for the largest, are dispersed into domains composed of numerous submicronic grains, 60 pct in area (Figure 1(b)). The so-called abnormal growth or its related partial recrystallization is competing with dislocation and point defects recovery that takes place during annealing. Moreover, precipitation is supposed to be heterogeneous, mainly because of these point and linear defects generated by mechanical alloying.[16] Thus, occurrence of grain growth and precipitation are strongly linked to diffusion kinetics and depend upon consolidation kinetics. Two main kinds of precipitates were found in sintered samples.

(a) Coarse Ti-enriched oxides not only aligned at grain boundaries but also present in the largest grains were systematically observed (Figure 1(b)). These lines may describe ex free surfaces of powder particles before compaction. Indeed, the mean distance between aligned precipitates, 10–40 μm, is the typical size of subparts of these granules, footprint of successive fracture, and cold welding during attrition milling.[17] Owing to their size and associated low number density, they most likely do not have any pinning effect on grain boundaries.

(b) Nanometric clusters detected by SANS. Experimental data were fitted assuming Gaussian size distributions of spherical particles,[18] giving rise to a high density of nanoclusters -1.4×10^{24} m^{-3}—with a mean radius of 1.4 nm, most likely Y-Ti oxides.[14,18] This also means that precipitation kinetic occurs very rapidly and mainly during the heating stage. A complete description of the precipitation kinetics will be described elsewhere.

To observe the influence of this heterogeneous microstructure on strength and ductility, tensile properties of the compacted sample were determined at various temperatures, as reported in Figure 2. The measured room temperature yield strength and ultimate tensile strength are 975 and 1054 MPa, respectively. First of all, these results demonstrate that an important improvement of the tensile strength at room temperature has been achieved when comparing with a previous study of SPS compaction.[19] Indeed, with a 2-step compaction followed by heat-treating, Sun *et al.* spark plasma sintered an ODS steel powder elaborated *via* sol–gel process. Yield strength at room temperature was 585 MPa (Figure 3). Even if no grain size was mentioned, one can expect that the sol–gel method does not produce nanocrystalline powder, contrary to high-energy milling. Thus, hardening due to grain size and defects density is very limited. Yield strength at room temperature is

Table I. Composition (Wt Pct) of Mechanically Alloyed Powder and Sintered Sample Measured by Electron Probe Microanalysis

Element	Fe	Cr	W	Y	O	Ti	Si
Powder, Ref.	bal.	14.6	0.99	0.16	0.15	0.32	0.19
Sintered Sample	bal.	14.5	1.01	0.16	0.15	0.32	0.18

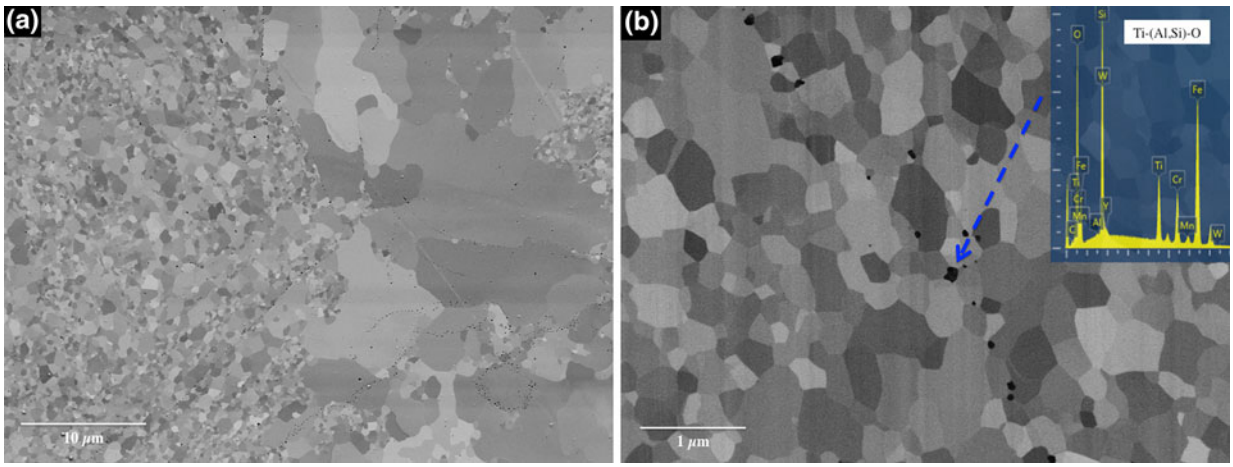

Fig. 1—SEM-FEG image of the heterogeneous microstructure of ODS steel compacted by SPS at 1373 K (1100 °C) (*a*) and Ti-enriched oxides at submicronic grain boundaries (*b*).

higher for SPSed materials when comparing to a 4-hour hot isostatic pressured steel (YS of 823 MPa), whereas the two processes tend to induce the same results at high temperature.[20,21] Higher tensile strength of extruded steel is likely related to the powder compaction mechanisms that induce strong work hardening through high density of dislocations and point defects.[22–24] Thus, hardening caused by dislocation forest is expected to be lower in recovered SPSed materials. Yet, as the process induces a very dense and fine nano-oxides dispersion within the ferritic matrix, Orowan strengthening through by-passing of nanoparticles is highly probable at room temperature, as demonstrated by Takahashi *et al.*[25] and Steckmeyer *et al.*[26] It is worth noticing that the mechanical behavior of SPSed materials is isotropic regarding both tensile strength and total elongation, not only at room temperature but also at 923 K (650 °C). This contrasts with what is usually observed on extruded ferritic steels.[27] For example, Fe-13.5Cr ODS steels produced by mechanically alloying and HE at 1373 K (1100 °C) led to an anisotropy ratio between total elongations in transverse and axial directions of 0.3 and 0.4, at room temperature and at 873 K (600 °C), respectively.[23] Based on the same criteria, SPSed ODS steel anisotropy ratios are 0.8 at room temperature and 1 at 923 K (650 °C). As tensile specimen geometry/thickness may have a role on strain-softening behavior,[28] it is worth noticing that isotropy is observed on both uniform and total elongation.

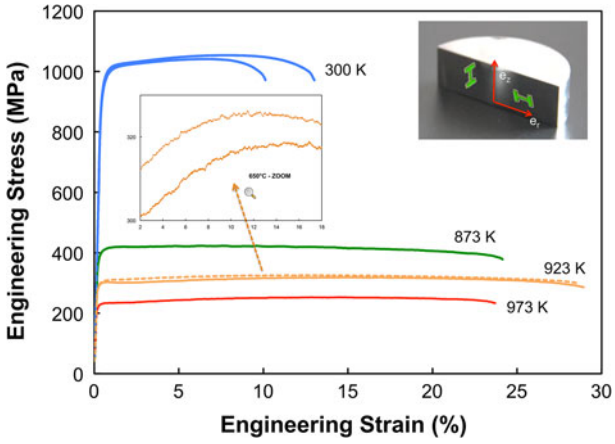

Fig. 2—Tensile properties under axial (plain lines) and radial (dash lines) directions at room and high temperature.

Fractographic examinations of tensile specimen are reported on Figure 4. The fracture surface is essentially covered by dimpled features, characteristic of ductile behavior. It shows various degrees of ductility, noted by the dispersion in the size of the microvoids formed during necking. This was observed in a scattered way across the surface of the fractured specimen and can be a manifestation of the abnormal grain growth shown in Figure 1. This connection between heterogeneous grain structure and dimpled surface has already been reported on nanocrystalline Cu-Nb prepared by mechanical alloying and HE.[29] However, double population of precipitates acting as brittle phases should play a significant role on fracture.[30] Finer observations on the samples machined along the axial direction—meaning the loading direction during compaction—revealed spare cleavage zones at room temperature. Several crack paths were identified on brittle zones. The latter were running through interface between powder granules, size of which varied from 1 to 50 μm. This type of intergranular and transgranular cleavages was also reported on sintered Fe-Al powder.[31] This highlights the interest of reducing the processing artefacts responsible for ductility loss, as shown on bulk nanostructured Nickel.[32]

In this sense, one-step compaction by SPS can be an answer. Most importantly, heterogeneous grain distribution with ultrafine (100 nm $< d <$ 1 μm) and larger grains seems to be a good compromise for strength and ductility.[33] Small grains, as in pure nanocrystalline metals, induce outstanding strength when grains large enough to favor dislocation activity can provide substantial strain-hardening, therefore boosted ductility.[34] This statement is of primary interest as abnormal grain growth systematically occurs during SPS consolidations above 1323 K (1050 °C). Thus, the ratio of

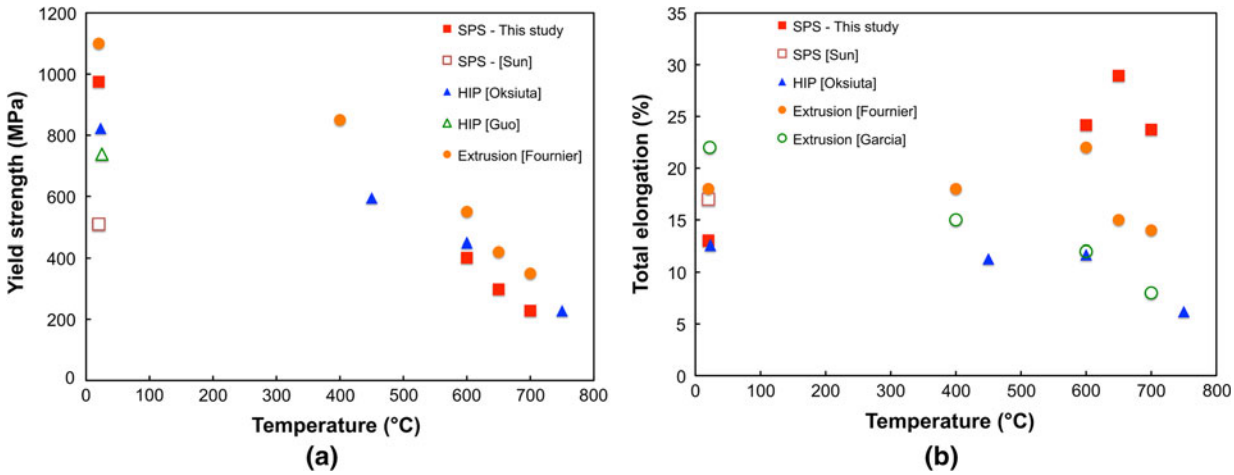

Fig. 3—Yield strength (*a*) and total elongation (*b*) of SPSed ODS steels, compared with other Fe-14Cr ODS consolidated by SPS, HIP and HE.

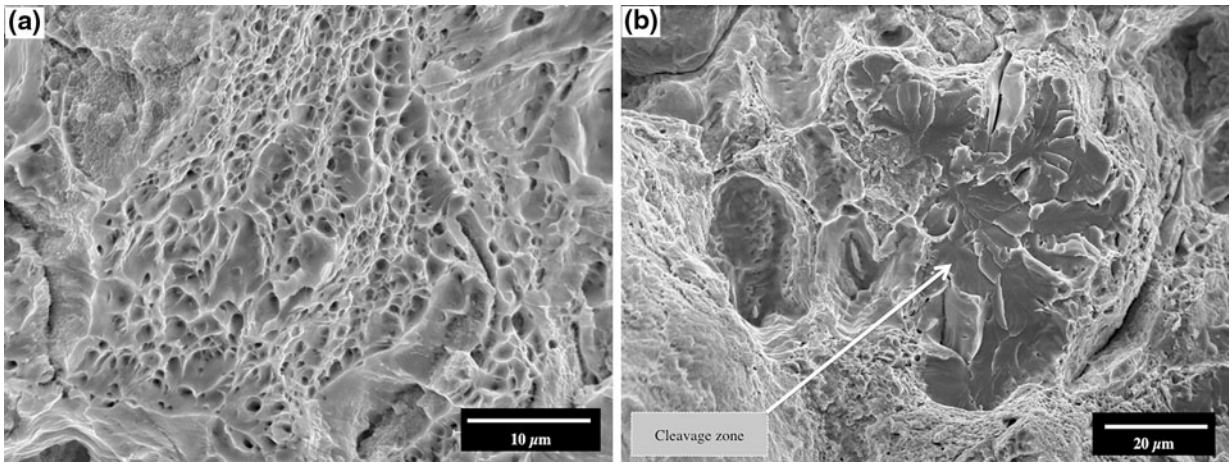

Fig. 4—SEM images of fractured tensile specimen tested at room temperature along the axial direction.

ultrafine grained region to coarse-grained region is almost constant within a temperature range 1323 K to 1423 K (1050 °C to 1150 °C) and permits sufficient reproducibility of the tensile properties. This can be validated by the study of Grosdidier *et al.*[12] which states that getting hetero-nanostructured ODS FeAl results from the combination of local heating during SPS processing and the use of heavily cold-worked milled powders.

In conclusion, dense ODS steels were elaborated by SPS at 1373 K (1100 °C) in less than 20 minutes. Due to high density of defects induced by mechanical alloying, nanocrystalline structure undergoes abnormal growth, leading to a fine and heterogeneous grain structure. Because of its ability to quickly heat up the powder, SPS allows to retain the major part of the submicronic grains, surrounded by larger grains. This specific microstructure is most likely responsible for: (1) High tensile strength induced by small grains—some are still substructured and deformed—and high density of fine complex nano-oxides. (2) Excellent ductility, especially because larger grains can accept decent work-hardening. However, other plasticity mechanisms at high temperature, such as superplasticity, may occur. Indeed, grain boundary sliding (GBS) involving ultrafine grains was observed to play a significant role on strain-hardening.[35] Moreover, tensile properties are isotropic along the whole temperature range, suggesting no influence of texture in the materials. The current study demonstrates that SPS can be an efficient alternative processing route to produce dense ferritic steels with high tensile strength and very acceptable ductility.

The authors gratefully thank F. Mercier and G. Bonnefont for their assistance in SPS compaction and D. Hamon, P. Wident and A. Bougault for their contribution in materials characterization. The current study was performed with financial support of the French CNRS GdR GEDEPEON and for the MATTER project within the seventh European framework. The current study was made in the frame of a tripartite agreement between the CEA, AREVA NP, and EDF.

REFERENCES

1. S. Ukai, M. Harada, H. Okada, M. Inoue, S. Nomura, S. Shikakura, T. Nishida, M. Fujiwara, and K. Asabe: *J. Nucl. Mater.*, 1993, vol. 204, pp. 65–73.
2. S. Ukai and M. Fujiwara: *J. Nucl. Mater.*, 2002, vols. 307–311, pp. 749–57.
3. R.L. Klueh, D.S. Gelles, S. Jitsukawa, A. Kimura, G.R. Odette B. van der Schaaf, and M. Victoria: *J. Nucl. Mater.*, 2002, vols. 307–311, pp. 455–65.
4. M.J. Alinger, G.R. Odette, and D.T. Hoelzer: *Acta Mater.*, 2009, vol. 57, pp. 392–406.
5. Y. De Carlan, J.L. Béchade, P. Dubuisson, J.L. Seran, P. Billot A. Bougault, T. Cozzika, S. Doriot, D. Hamon, J. Henry, M. Ratti, N. Lochet, D. Nunes, P. Olier, T. Leblond, and M.H. Mathon: *J. Nucl. Mater.*, 2009, vols. 386–388, pp. 430–32.
6. P. Dubuisson, Y. de Carlan, V. Garat, and M. Blat: *J. Nucl. Mater.*, 2012, vol. 428, pp. 6–12.
7. S. Saroja, A. Dasgupta, and R. Divakar: *J.Nucl. Mater.*, 2011, vol. 4009, pp. 131–39.
8. M. Wang, Z. Zhou, H. Sun, H. Hu, and S. Li: *Mater. Sci. Eng., A*, 2013, vol. 559, pp. 287–92.
9. W.M. Guo, Z.G. Yang, and G.J. Zhang: *Int. J. Refract. Met. Hard Mater.*, 2011, vol. 29, pp. 452–55.
10. D. Fabrègue, J. Piallat, E. Maire, Y. Jorand, V. Massardier-Jourdan, and G. Bonnefont: *Powder Metall.*, 2012, vol. 55, pp. 76–79.
11. R. Orru, R. Licheri, M. Locci, A. Cincotti, and G. Cao: *Mater. Sci. Eng. R*, 2009, vol. 63, pp. 127–287.
12. T. Grosdidier, G. Ji, and S. Launois: *Scripta Mater.*, 2007, vol. 57, pp. 525–28.
13. G. Ji, T. Grosdidier, N. Bozzolo, and S. Launois: *Intermetallics*, 2007, vol. 15, pp. 108–18.
14. M. Ratti, D. Leuvrey, M.H. Mathon, and Y. de Carlan: *J. Nucl. Mater.*, 2009, vols. 386–388, pp. 540–43.
15. L. Toualbi, M. Ratti, G. André, F. Onimus, and Y. de Carlan: *J. Nucl. Mater.*, 2011, vol. 417, pp. 225–28.
16. A. Molinari, S. Libardi, M. Leoni, and P. Scardi: *Acta Mater.*, 2010, vol. 58, pp. 963–66.
17. D. Bouvard: *Métallurgie des poudres*, Mim, Édition Hermes-Lavoisier, Paris, 2002.

18. M.H. Mathon, M. Perrut, S.Y. Zhong, and Y. de Carlan: *J. Nucl. Mater*., 2012, vol. 428, pp. 147–53.
19. Q.X. Sun, T. Zhang, X.P. Wang, Q.F. Fang, T. Hao, and C.S. Liu: *J. Nucl. Mater*., 2012, vol. 424, pp. 279–84.
20. Z. Oksiuta, P. Mueller, P. Spätig, and N. Baluc: *J. Nucl. Mater*., 2011, vol. 412, pp. 221–26.
21. L. Guo, C. Jia, B. Hu, and H. Li: *Mater. Sci. Eng. A*, 2010, vol. 527, pp. 5220–24.
22. A. Garcia-Juncedan, M. Hernandez-Mayoral, and M. Serrano: *Mater. Sci. Eng. A*, 2012, vol. 556, pp. 696–703.
23. B. Fournier, A. Steckmeyer, A.-L. Rouffie, J. Malaplate, J. Garnier, M. Ratti, P. Wident, L. Ziolek, I. Tournie, V. Rabeau, J.M. Gentzbittel, T. Kruml, and I. Kubena: *J. Nucl. Mater*., 2012, vol. 430, pp. 142–49.
24. P. Unifantowicza, Z. Oksiuta, P. Olier, Y. De Carlan, and N. Baluc: *Fusion Eng. Des*., 2011, vol. 86, pp. 2413–16.
25. A. Takahashi, Z. Chen, N. Ghoniem, and N. Kioussis: *J. Nucl. Mater*., 2011, vol. 417, pp. 1098–101.
26. A. Steckmeyer, M. Praud, B. Fournier, J. Malaplate, J. Garnier J.L. Béchade, I. Tournié, A. Tancray, A. Bougault, and P. Bonnaillie: *J. Nucl. Mater*., 2010, vol. 405, pp. 95–100.
27. R. Kasada, S.G. Lee, J. Isselin, J.H. Lee, T. Omura, A. Kimura T. Okuda, M. Inoue, S. Ukai, S. Ohnuki, T. Fujisawa, and F. Abe: *J. Nucl. Mater*., 2011, vol. 417, pp. 180–84.
28. Y.H. Zhao, Y.Z. Guo, Q. Wei, A.M. Dangelewicz, C. Xu, Y.T. Zhu, T.G. Langdon, Y.Z. Zhou, and E.J. Lavernia: *Scripta Mater*., 2008, vol. 59, pp. 627–30.
29. K.A. Darling, B.G. Butler, H.E. Maupin, L.J. Kecskes, and S.N. Mathaudhu: *Proceedings of the 2012 International Conference on Powder Metallurgy & Particulate Materials*, Las Vegas, NV, pp. 0929–0939.
30. D. Fabrègue and T. Pardoen: *J. Mech. Phys. Solids*., 2008, vol. 56 (3), pp. 719–41.
31. G. Ji, F. Bernard, S. Launois, and T. Grosdidier: *Mater. Sci. Eng. A*, 2013, vol. 559, pp. 566–73.
32. Y. Zhao, T. Topping, J.F. Bingert, J. Thornton, A.M. Dangelewicz, and Y. Li: *Adv. Mater*., 2008, vol. 20, pp. 3028–33.
33. C.C. Koch: *Scripta Mater*., 2003, vol. 49, pp. 657–62.
34. Y. Wang, M. Chen, F. Zhou, and E. Ma: *Nature*, 2002, vol. 419, pp. 912–15.
35. A.K. Mukherjee: *Mater. Sci. Eng. A*, 2002, vol. 322, pp. 1–22.